Mon. Not. R. Astron. Soc. **000**, 1–14 (2003) Printed 15 April 2004 (MN LaTeX style file v2.2)

High resolution imaging of the radio continuum and neutral gas in the inner kiloparsec of the radio galaxy 3C 293

R. J. Beswick,[1⋆] A. B. Peck,[2] G. B. Taylor[3] and G. Giovannini[4]

1. The University of Manchester, Jodrell Bank Observatory, Macclesfield, Cheshire SK11 9DL, UK
2. Harvard-Smithsonian Center for Astrophysics, SAO/SMA Project, P.O. Box 824, Hilo, HI 96721
3. National Radio Astronomy Observatory, P.O. Box O, Socorro, NM 87801
4. Istituto di Radioastronomia del CNR, via Gobetti 101, 40129 Bologna, Italy

Accepted 29/03/04

ABSTRACT

Using a combination of observations involving the VLA, MERLIN and global VLBI networks we have made a detailed study of the radio continuum and the neutral hydrogen (HI) kinematics and distribution within the central kiloparsec of the radio galaxy 3C 293. These observations trace the complex jet structure and identify the position of the steeply inverted radio core at 1.3 GHz.

Strong HI absorption is detected against the majority of the inner kiloparsec of 3C 293. This absorption is separated into two dynamically different and spatially resolved systems. Against the eastern part of the inner radio jet narrow HI absorption is detected and shown to have higher optical depths in areas co-spatial with a central dust lane. Additionally, this narrow line is shown to follow a velocity gradient of $\sim$50 km s^{-1} arcsec^{-1}, consistent with the velocity gradient observed in optical spectroscopy of ionised gas. We conclude that the narrow HI absorption, dust and ionised gas are physically associated and situated several kiloparsecs from the centre of the host galaxy. Against the western jet emission and core component, broad and complex HI absorption is detected. This broad and complex absorption structure is discussed in terms of two possible interpretations for the gas kinematics observed. We explore the possibility that these broad, double absorption spectra are the result of two gas layers at different velocities and distances along these lines of sight. A second plausible explanation for this absorbing structure is that the HI is situated in rotation about the core of this radio galaxy with some velocity dispersion resulting from in-fall and outflow of gas from the core region. If the latter explanation were correct, then the mass enclosed by the rotating disk would be at least 1.7×10^9 solar masses within a radius of 400 pc.

Key words: galaxies: individual: 3C293 – Radio lines: galaxies – galaxies: Radio – galaxies: active

1 INTRODUCTION

Nuclear activity in galaxies manifests itself in a variety of forms from nearby low luminosity active galactic nuclei (AGN), such as Seyferts and LINERS, to powerful distant quasars and radio galaxies. In these sources, the nuclear activity is responsible for radiation detected across the entire electromagnetic spectrum. In the radio loud active galaxies, such as quasars and radio galaxies, the radio emission demonstrates the influence of the AGN, for example via the formation of powerful jets (Fanaroff & Riley 1974). Additionally ample evidence is also available from other wavelength ranges (*e.g* optical) for the interaction of the nuclear activity with the surrounding galactic interstellar medium (ISM) such as via the detection of outflows from nuclear regions of some Seyfert galaxies (*e.g.* NGC 3079, Cecil et al. 2001). The commonly accepted standard model for nuclear activity asserts that the AGN is fuelled by the release of gravitational potential energy as galactic material is accreted onto a central super-massive black hole. As such

⋆ rbeswick@jb.man.ac.uk

© 2003 RAS

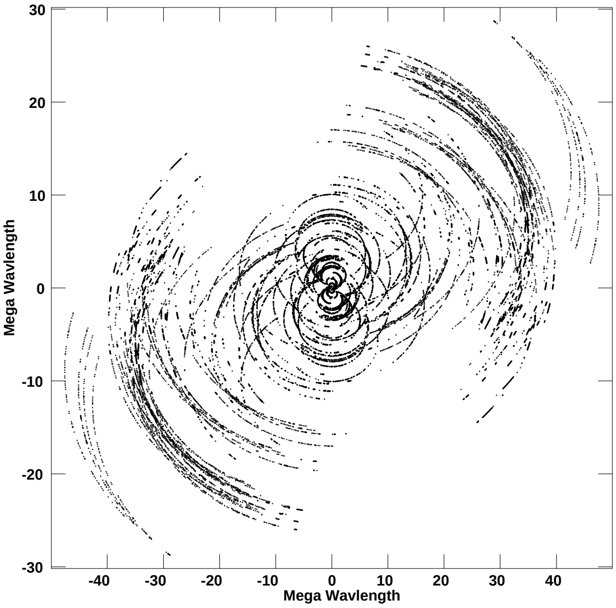

Figure 1. The *u-v* coverage of the combined VLBI and MERLIN data-sets.

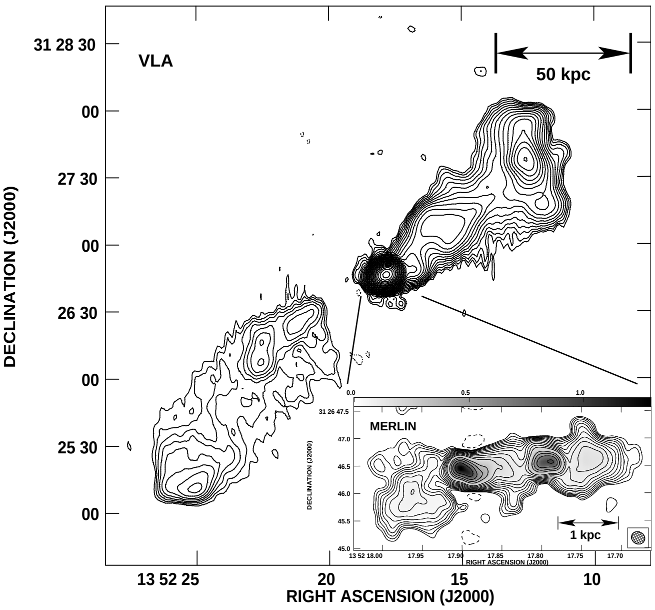

Figure 2. VLA B configuration image at 1.35 GHz of the large scale structure of the radio galaxy 3C 293 along with inset MERLIN image of the central ∼3 kpc. The VLA image has been contoured at $\sqrt{2}$ times 0.5 mJy beam^{-1} with a peak flux of 3.44 Jy. The lowest contour of the inset MERLIN image is 5 mJy beam^{-1} and follows the same multiplying factors as the VLA image. The peak of the MERLIN image is 1.29 Jy beam^{-1}. The MERLIN radio continuum image can be seen in more detail in Fig. 2.

Table 1. Summary of Observations. All three of these observations were made in spectral line mode with the bandwidth centred at 1.359 GHz.

Interferometer	Date	BW (MHz)	*uv* Range (kλ)
VLA-A+PT	15/12/2000	3.125	3.1-235
MERLIN	08/04/1998	8	11-989
VLBI	18/11/1999	8	162-4850

it is incumbent upon investigators to study not only the effects of this nuclear activity (*e.g.* jets) but also the physical and kinematic environment that surrounds the AGN, since this provides a method by which we can study how gas, dust and stars act as fuel for the activity we observe as well as how this activity impacts the surrounding ISM.

At the present time most high angular resolution studies of powerful active galaxies have concentrated upon investigating the consequences of the activity (*e.g.* the synchrotron emission such as radio jets), rather than the cause of the activity (*e.g.* cold neutral and molecular gas that fuels the nuclear activity). This has primarily been a direct consequence of observational constraints resulting from the relatively small collecting areas of the current generation of mm-wavelength aperture synthesis instruments and the surface brightness sensitivity of decimetre wavelength interferometers precluding observations of cold thermal gas emission at angular resolutions of $\lesssim$1 arcsec. However using current radio aperture synthesis techniques it is possible to observe cold gas, via decimetre transitions such as HI, OH and H_2CO, in absorption against the bright background radio continuum of some galaxies, on sub-arsecond angular scales.

3C 293 is a nearby radio galaxy associated with the peculiar elliptical galaxy VV5-33-12. On scales of several tens of kiloparsecs, the radio jet structure of 3C 293 has been well studied by Bridle, Fomalont & Cornwell (1981) and van Breugel et al. (1984) and resembles a moderately large two-sided FR-II radio galaxy. However, 3C 293 is peculiar in that an unusually high proportion of the galaxy's radio power is emitted from a steep-spectrum extended core component. This core region when observed at higher angular resolution, is found to be a composite of several radio components forming a kiloparsec scale east-west orientated jet (Bridle et al. 1981; Akujor et al. 1996; Beswick, Pedlar & Holloway 2002). At other wavelengths, 3C 293 and its associated galaxy display several distinctive characteristics. VV5-33-12 has a closely interacting small companion galaxy situated ∼37″ (∼30 kpc) toward the south-west (Heckman et al. 1985; Evans et al. 1999) and the central region of the galaxy is criss-crossed by several filamentary dust lanes aligned in an approximately north-south direction (van Breugel et al. 1981; Martel el. 1999; Allen et al. 2002). Additionally *Hubble Space Telescope* (*HST*) observations have detected an optical/IR jet within the central kiloparsec (Leahy, Sparks & Jackson 1999) partially obscured from previous observations by the nuclear dust lanes. Arcsecond resolution observations of molecular gas in 3C 293 by Evans et al. (1999) have revealed large concentrations of CO(1→0) detected in both emission and absorption within the central few kiloparsecs. The CO emission is primarily distributed in an asymmetric disk rotating about an unresolved continuum component that Evans et al. conclude is the AGN.

Broad neutral hydrogen absorption was first detected against 3C 293 by Baan & Haschick (1981) using the Arecibo telescope and has been studied in great detail with ever improving sensitivities and angular resolutions using a variety of radio interferometers over the last two decades (Shostak et al. 1983; Haschick & Baan 1985; Beswick et al. 2002; Morganti et al. 2003). 3C 293 has proved to be worthy of these numerous studies because of its complex and exceptionally broad HI absorption structure which has been observed against the extended nuclear radio continuum source. In order to fully sample the wide range of physical scales of the nuclear radio continuum of 3C 293 from several arcseconds to angular resolutions of a few tens of mas we have combined global Very Long Baseline Interferometry (VLBI) observations with previously published Multi-Element Radio Linked Interferometric Network (MERLIN) data (Beswick et al. 2002) and Very Large Array (VLA: A configuration including the VLBA Pie Town antenna) observations to provide a wide range of *u-v* spacings (see Tab. 1 and Fig. 1). This combined study allows this extended radio source to be imaged with high fidelity at a variety of angular resolutions.

This paper is split into four additional sections. The first of these will describe the observations presented and the data processing that has been applied to them. This will be followed by the presentation of the observational results and a more detailed discussion of their implications. The discussion will initially concentrate upon the radio continuum structure of 3C 293 from arcmin to milliarcsec scales, comparing these new observations with previously published data-sets, followed by a detailed discussion of these new mas resolution HI absorption observations against the central kiloparsec of 3C 293. The final section of this paper will outline the key conclusions of this work and place them in context of other radio galaxies and their environments.

Throughout this paper we assume $H_0 = 75\,\mathrm{km\,s^{-1}\,Mpc^{-1}}$. At a redshift of z=0.045 this implies a distance for 3C 293 of 180 Mpc so an angular size of 1 mas corresponds to 0.815 pc.

2 OBSERVATIONS & IMAGE PROCESSING

2.1 VLA plus Pie Town Observations

Observations centred at 1359.518 MHz were taken with the VLA on December 15$^{\mathrm{th}}$ 2000 in A configuration using 64 channels across a bandwidth of 3.125 MHz. Data from both right and left circular polarizations were obtained. The VLBA antenna at Pie Town also participated in the observations and the IF signal was distributed to the VLA correlator via a Western New Mexico Telephone Co. fibre optic link. A single VLA antenna was removed from the array so that its place in the electronics could be used by the Pie Town antenna. The length of the observing run was 8 hours. The strong calibrator 3C286 was employed for bandpass and absolute flux calibration.

2.2 MERLIN Observations

3C 293 was observed with the UK MERLIN array (Thomasson 1986) with 7 telescopes on April 8$^{\mathrm{th}}$ 1998. The observations measured both left and right hands of polarization across an 8 MHz bandwidth centred upon the redshifted frequency of the HI line in 3C 293 (1359 MHz). These data were correlated into 64 frequency channels of width 125 kHz (28.8 $\mathrm{km\,s^{-1}}$). These observations were made over a period of 18 hours and were phase and bandpass calibrated using observations of the source OQ208 which were regularly interspersed throughout the observing run. An observation of 3C 286 at either end of the observing run was used to calibrate the absolute flux density scale for all the MERLIN observations. Initial calibration and editing of this data-set were made at Jodrell Bank using local MERLIN software routines. Following this, these data were imported into AIPS where further editing and calibration values were derived and applied using phase solutions obtained from the phase calibration source OQ208 and using standard self-calibration techniques. The observations and processing of the MERLIN data-set have been described in more detail in Beswick et al. (2002) and Beswick (2002).

2.3 VLBI Observations

Global VLBI observations made with the European VLBI Network (EVN) antennas at Westerbork, Onsala, Medicina, and Effelsberg, the VLBA, and the phased VLA were obtained on November 18$^{\mathrm{th}}$ 1999. The VLBA correlator in Socorro produced 512 spectral channels across a bandwidth of 8 MHz centred at 1359.29 MHz. Four level sampling was used and data from both right and left circular polarizations were processed. Delay, rate and amplitude calibration were obtained from short (4 min) observations of OQ208 obtained every $\sim$30 min. The length of the observing run was 14 hours. Bandpass calibration was obtained from observations of the strong calibrator 3C345.

2.4 Combination of these three data-sets

Initial phase and amplitude calibration was done on each data-set independently, using OQ208 in all cases, as described above. The MERLIN data were then shifted to J2000 coordinates to match the other data-sets. The global VLBI data and VLA+PT data were averaged in frequency to correspond with the lower velocity resolution MERLIN data, and the central frequencies were shifted slightly so that the frequency range and channel numbers in all data-sets matched exactly. The data-sets were then concatenated by combining the VLA+PT and MERLIN data, and then the VLBI data, with iterations of self-calibration at each stage. The relative weights for the data from each array were also checked during the process. The combined data were subsequently Fourier transformed and deconvolved using a circular 30 mas restoring beam to form a 2048$\times$2048$\times$23 spectral line cube to which standard spectral line routines within AIPS were applied.

The primary benefit of combining these data-sets is that it allows the final image created from the radio interferometric data to sample a wide range of angular size scales and thus give a more complete representation of the radio emission. The combined image with 30 mas angular resolution contains a total flux density of 3.2 Jy compared with the total flux density of 9.8 Jy derived from the 200 mas angular resolution MERLIN image. The missing flux density in the higher angular resolution combined image results from spatial filtering of the more diffuse structures which are seen in the MERLIN image.

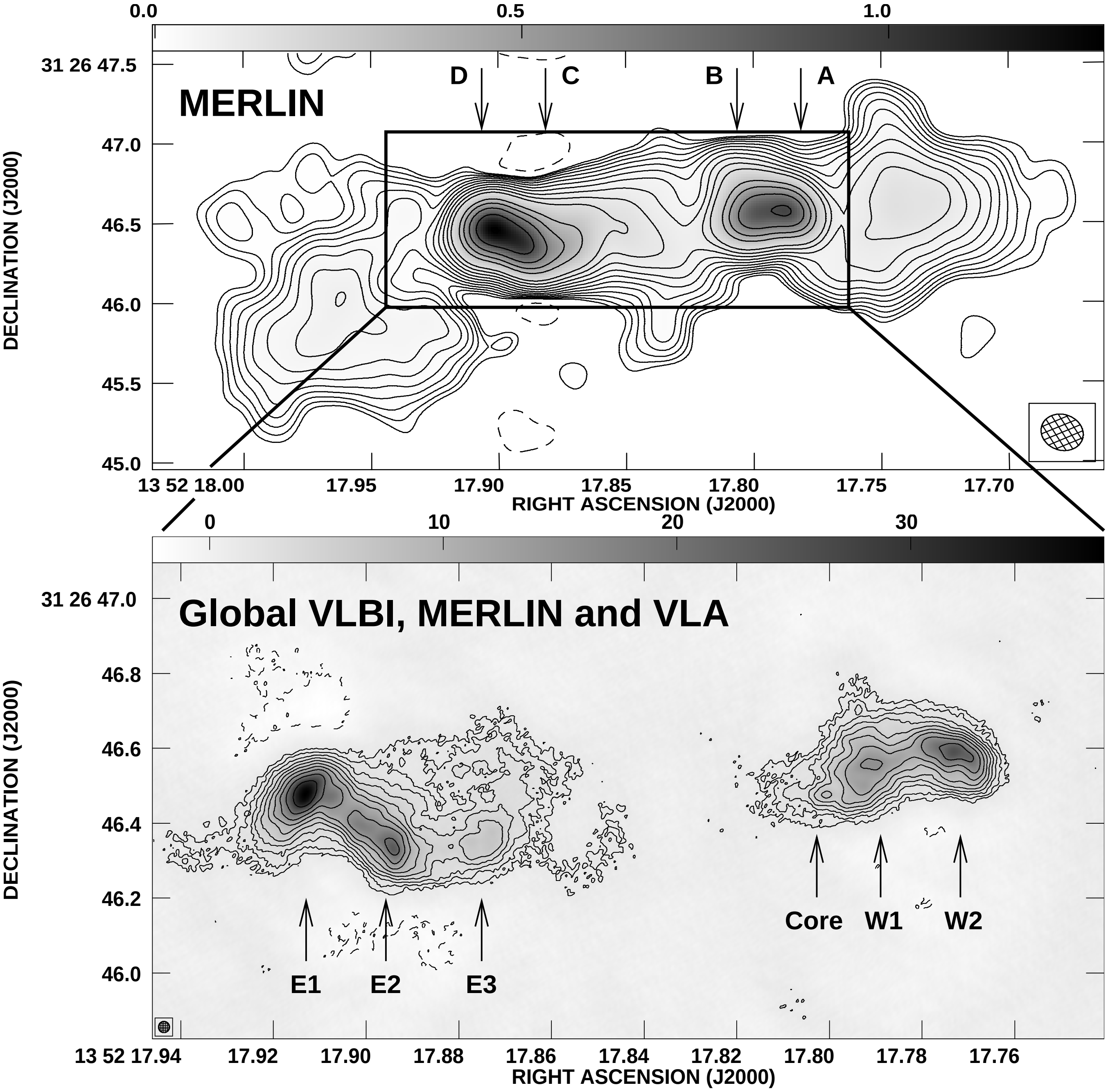

Figure 3. Sub-arcsecond continuum structure of the inner few kiloparsecs of 3C 293. The top contour map shows the 1.359 GHz radio continuum structure observed with MERLIN at a resolution of 0.″23×0.″20. Contour levels of the MERLIN image are the same as for Fig. 1. The lower panel shows the global VLBI, MERLIN and VLA+PT contoured image of the inner jet of 3C 293 with angular resolution of 30 mas. This map is contoured at multiples of $\sqrt{2}$ times 1.3 mJy beam^{-1}. The peak flux of the 30 mas image is 38.23 mJy. Labels A, B, C and D at the top of the MERLIN image follow the convention of labeling continuum components in this source used by Bridle et al. (1981) and Beswick et al. (2002).

3 RESULTS

3.1 Multi-scale radio continuum emission

The large scale radio continuum structure of 3C 293 is shown in Fig. 2. This image was formed from VLA B-configuration data obtained as part of the global VLBI observations and shows the large double jet/lobe structure of the FR-II radio galaxy 3C 293. The radio continuum structure of 3C 293 upon these angular scales consists of a wide two-sided radio jet/lobe extending approximately 90 arcsec at a P.A.$\sim$45° with a bright central radio core of peak flux density 3.44 Jy. The radio continuum structure of 3C 293 upon these large scales shows the north-western radio jet and lobe to have a significantly larger radio flux than the south-eastern jet, consistent with the north-western jet approaching upon these scales. The inset image in Fig. 2 shows the naturally weighted (0.″23×0.″20 angular resolution) MERLIN image of the central core region. This image, formed from the absorp-

Table 2. Spectral indices between 1.359 and 4.546 GHz[1] for components in the inner jet. Flux densities for both frequencies have been obtained from matched angular resolution (50 mas) images. Positions of components have been derived from the 1.359 GHz image presented pictorially in Fig. 2, bracketed labels equivalent to the position labels of the spectra in Fig. 3 & 4 and Tab. 3. The flux densities quoted are for the peaks for each radio continuum component at both frequencies in addition to the integrated flux density of each component. Spectral indices have been calculated using $S_\nu \propto \nu^{-\alpha}$.

Component	RA (J2000) $13^h\,52^m$	Dec (J2000) $31°\,26'$	$S_{1.359GHz}$ Peak (mJy beam^{-1})	$S_{1.359GHz}$ Total (mJy)	$S_{4.546GHz}$ Peak (mJy beam^{-1})	$S_{4.546GHz}$ Total (mJy)	Spectral Index $\alpha^{1.3}_{4.5}$
E1(2)	$17^s.913$	$46''.48$	90.48	564.13	55.00	256.25	0.65
E2(5)	17.895	46.34	53.81	427.06	28.50	242.80	0.47
E3(6)	17.873	46.36	17.44	134.10	10.42	67.69	0.57
Core(7)	17.800	46.48	16.38	27.10	20.87	23.55	0.11
W1(8)	17.791	46.56	38.52	460.69	9.60	133.38	1.03
W2(11)	17.773	46.59	59.13	484.60	25.84	214.67	0.67

tion free continuum channels of the MERLIN data-set (see Beswick et al. 2002 for details of this observation), shows the structure of the central 3 kpc of the radio jet of 3C 293. This central region of 3C 293 is resolved into several continuum components following an east-west orientation. The jet orientation between these two spatial scales deviates by nearly 45° as has been previously noted by Bridle et al. (1981), Evans et al. (1999) and Beswick et al. (2002).

At the $0''.2$ angular resolution of the MERLIN observations, the inner jet of 3C 293 shows at least four distinct radio components (labeled A, B, C & D in Fig. 3 following Bridle et al. 1981) with two more diffuse lobe-like components extending on either side of the central region. At this resolution and frequency it is unclear which radio continuum component is coincident with the AGN. The lower portion of Fig. 3 shows the radio continuum structure of the inner part of the MERLIN image. This continuum map, formed from the line-free portion of the combined global VLBI, MERLIN and VLA spectral line cube, has been convolved with a 30 mas circular restoring beam and has a noise level of 0.4 mJy beam^{-1}. In this high resolution image the inner kiloparsec of the radio jet in 3C 293 can be seen to deviate significantly from its east-west trajectory. The continuum components A, B, C & D which are barely resolved in the MERLIN image are composed of numerous compact, bright knots of radio emission tracing the path of the radio jet. This jet structure is consistent with the 50 mas resolution 5 GHz MERLIN results presented by Akujor et al. (1996). The differences between the 5 GHz image published by Akujor et al. (1996) and our higher resolution 1.3 GHz image result from differences in the spectral index of the various components that form the jet and the insensitivity to more diffuse structures of the MERLIN 5 GHz image presented by Akujor et al. due to sparseness of the MERLIN array and exacerbated by the loss of the Defford telescope during their observations. In particular, the weak 1.3 GHz radio continuum component at $13^h52^m17^s.800$, $31°26'46''.48$ is at the same position as the steeply inverted component identified by Akujor et al. as the radio core. Both these observations and those of Akujor et al. were phase referenced using the same nearby calibrator source providing good absolute positions which have been confirmed by fitting the positions of the bright inner hotspots (E1, E2 and W2) visible in both data sets. Consequently the estimated positional offsets of these to observations is less than 15 mas. The spectral indices between 1.359 and 4.546 GHz[1] and positions for each of the components labelled in the lower part of Fig. 3 are listed in Tab. 2, using $S_\nu \propto \nu^{-\alpha}$.

3.2 High resolution neutral hydrogen absorption observations

Using the combined global VLBI, MERLIN and VLA data-set neutral hydrogen absorption has been detected and resolved against the majority of the radio continuum structure observed at mas angular resolutions. Figures 4 & 5 show montages of selected HI absorption spectra extracted from the 30 mas angular resolution data-set taken from the regions indicated on the continuum images for both the eastern and western sections of the inner jet structure shown in Fig. 3. The noise levels on individual channels of the 30 mas resolution spectral line cube are ∼0.7 mJy beam^{-1}. The HI absorption line characteristics and the positions at which each of these 13 spectra occur are detailed in Tab. 3. Also in Tab. 3 the peak opacities and associated HI column densities have been quoted. The column densities have been calculated using $N_H = 1.823\times10^{20}\,\frac{T_{spin}}{100\,K}\int\tau\,dV$ and assuming a spin temperature of 100 K. It should be noted, however, that these values of N_H are likely to be lower limits in some physical situations, such as close to the nuclei of active galaxies or in outflows, where the gas spin temperature may be as large as a few 1000 K (Maloney, Hollenbach & Tielens 1996).

As a result of the combination of three HI absorption data-sets (Global VLBI, MERLIN and VLA plus Pie Town) covering a wide range of *u*-*v* spacings it is possible to image the HI absorption reliably over a variety of angular resolutions. Figure 6 shows contour images of nine individual velocity channels showing the position and velocity distribution of the HI absorption. In this figure the data-set has been convolved with a 50 mas circular beam in order to increase the signal to noise of the absorption in the individual channels. From Figs. 4, 5, & 6 it is clear that the velocity structure and line width of the HI absorption is significantly different against the the eastern and western sections of the radio source. Against the western part of the inner radio jet, the

[1] MERLIN 4.5 GHz data with 50 mas angular resolution has been used for this comparison. Access to these data has been kindly provided prior to publication by J. P. Leahy.

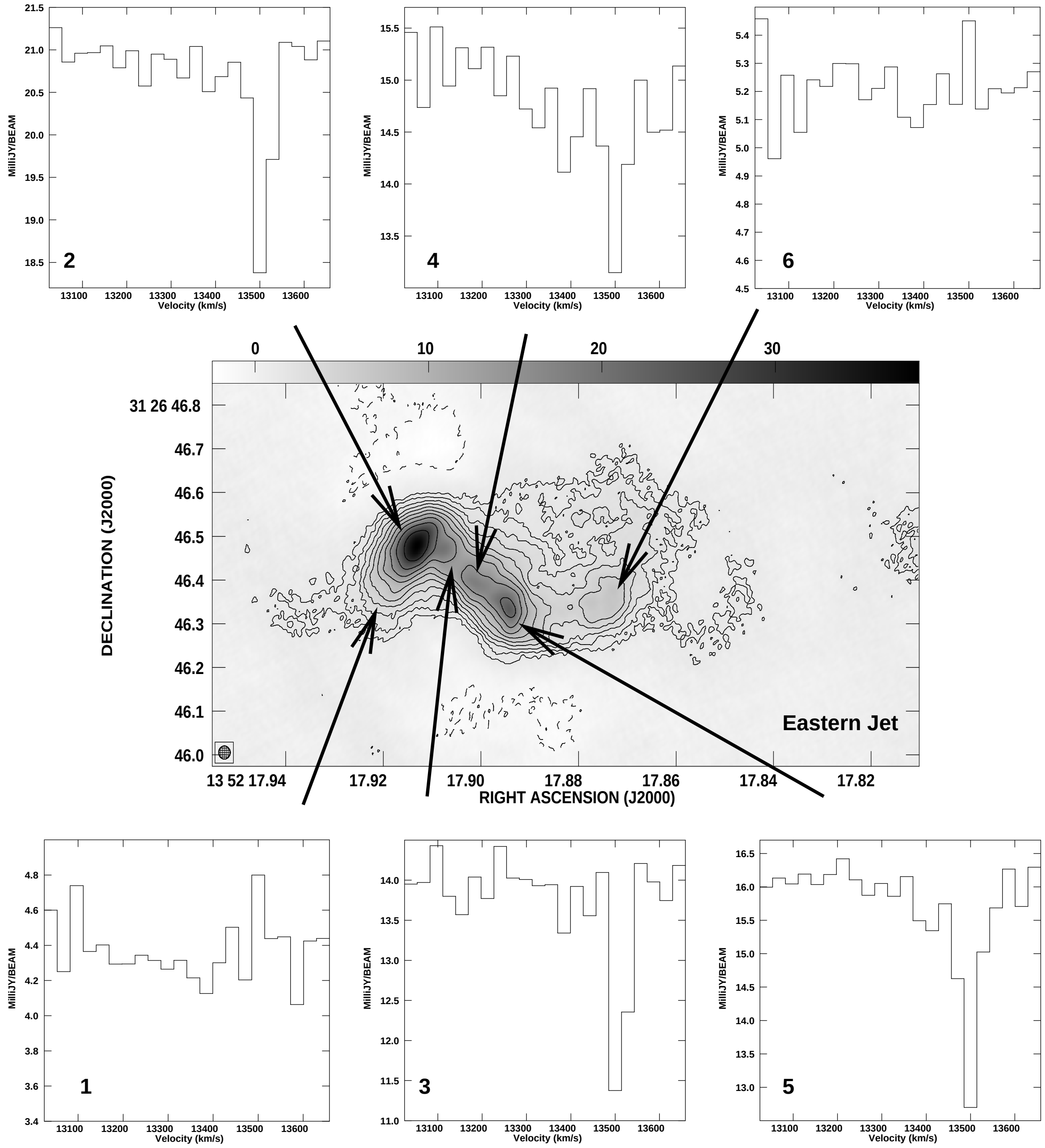

Figure 4. Montage of 1.35 GHz radio structure of the eastern part of the source with a 30 mas circular restoring beam along with selected Hi absorption spectra. Contours are identical to Fig. 3.

Hi absorption is significantly broader and weaker than the absorption observed against the eastern components. This is consistent with lower resolution Hi absorption observations of this source by Haschick & Baan (1985) with the VLA and by Beswick et al. (2002) with MERLIN.

The distribution of Hi optical depth and velocity toward the eastern components of the inner radio jet are shown in Fig. 7. In Fig. 7 the optical depths of the narrow Hi absorption against the eastern component are shown over the three spectral line channels that contain absorption significantly greater than the noise levels in individual channels. The spatial distribution of Hi in these three channels is consistent with a strip of foreground gas at an approximate PA of $\sim$35°. This strip of foreground gas is centred upon the rest velocity of 3C 293, 13 500 km s^{-1}, with a small south-west to north-east velocity gradient visible over the three channels.

Against the western half of the inner jet structure the Hi absorption is broader and generally composed of two or more velocity components (see Fig. 5). The complex velocity structure against this component is presented in Fig. 8 as three position velocity diagrams plotted as a function of R.A.. These diagrams have been formed by averaging the absorption signal convolved with three different restoring beams (80, 50 and 30 mas) over the declination range of the western radio jet component.

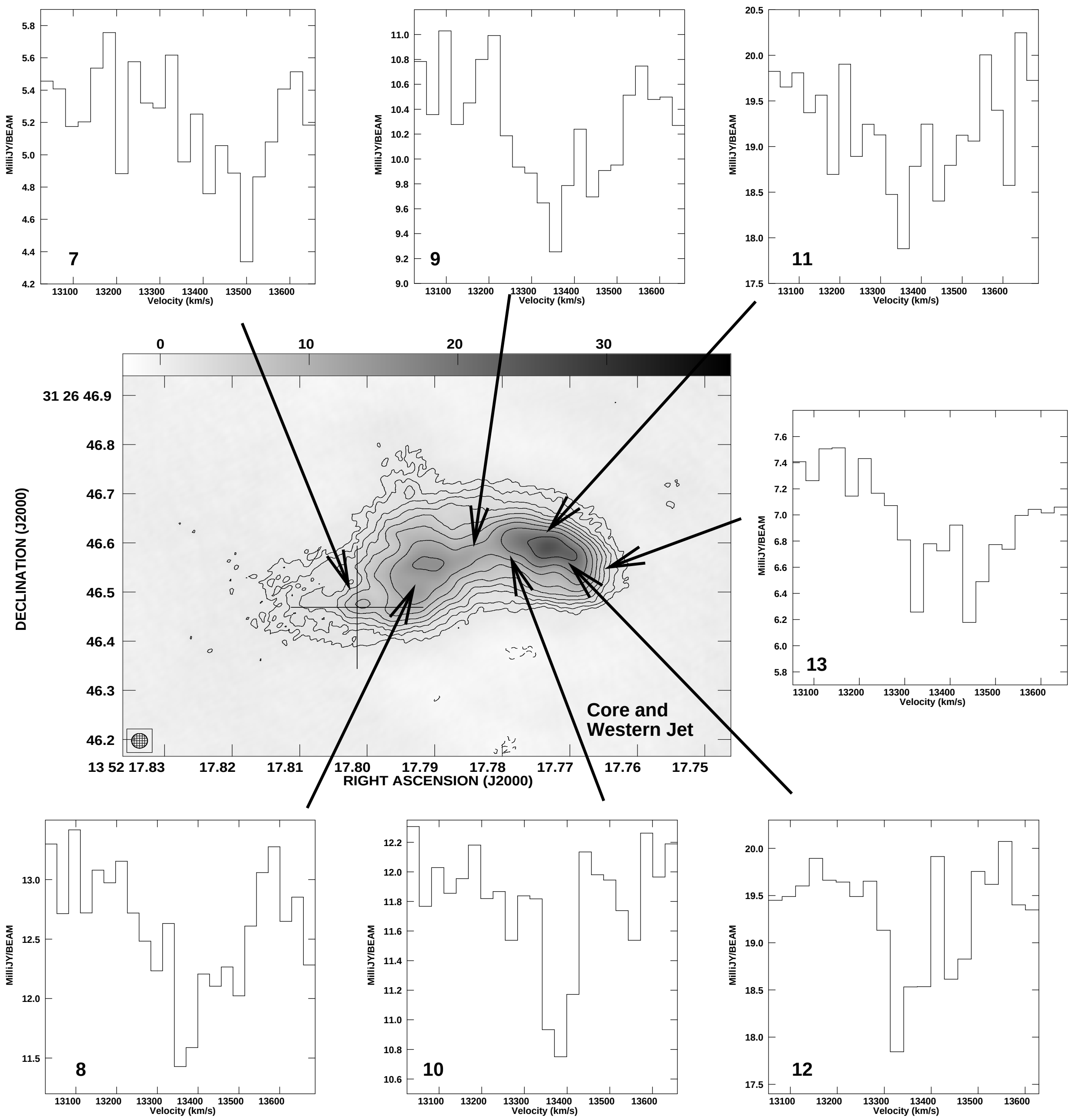

Figure 5. Montage of 1.35 GHz radio emission toward the western part of the source with a 30 mas circular restoring beam along with selected HI absorption spectra. Contours are identical to Fig. 3. The cross shown marks the position of the 5 GHz core detected by Akujor et al. (1996). The size of the cross is much larger than the relative astrometric error between the 5 GHz observations of Akujor et al. (1996) and the observations presented here.

4 THE RADIO CONTINUUM EMISSION

4.1 The location of the AGN at 1.3 GHz

In our previous sub-arcsecond MERLIN 1.3 GHz images of 3C 293 (Beswick et al. 2002), it was not possible to distinguish the core component from the extended radio continuum emission. However this source is well known to have a steeply inverted core, which consequently is clearly visible as an unresolved component in the 5 GHz MERLIN images presented by Akujor et al. (1996). Akujor et al. also found this component to be unpolarized at 22 GHz providing further supporting evidence that it is the nuclear component. The MERLIN 5 GHz position of this unresolved core identified as the nucleus is marked by a cross on Fig. 5 and listed in Tab. 2. At 1.3 GHz, this component is only separable from the extended radio continuum emission in our 30 mas angular resolution image and has a low flux density compared to the jet components within the image. Using Gaussian fitting techniques, Akujor et al. determine that the core component is unresolved with an angular size of $\lesssim$13 mas. A similar analysis of our 30 mas angular resolution, 1.3 GHz image also finds this component is unresolved with a deconvolved size of $\lesssim$20 mas implying a linear size of $\lesssim$17 pc.

The spectral index of the core between 1.359 GHz and

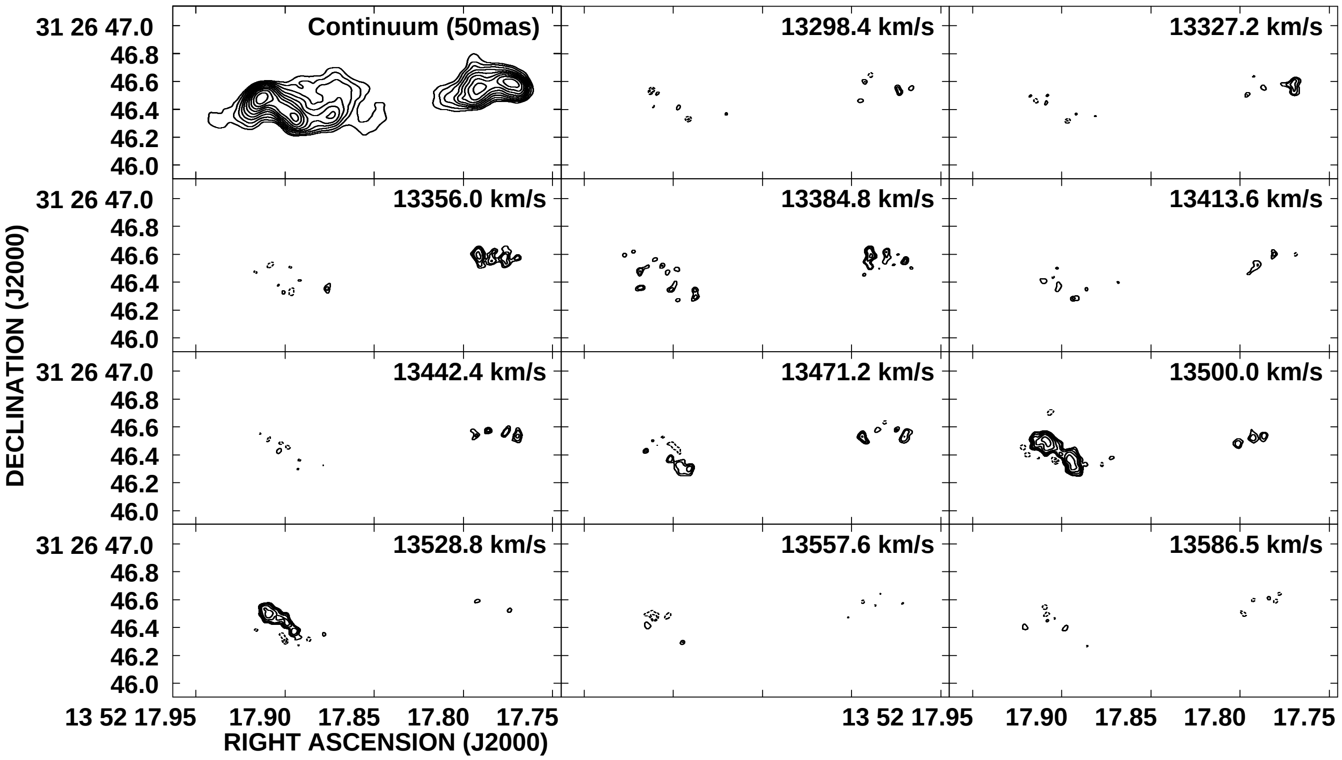

Figure 6. Nine individual channel maps of HI absorption across the inner kiloparsec of 3C 293 with an angular resolution of 50 mas. The contour levels mapping the absorption are −11.31, −8, −5.657, −4, −2.828, −2, −1.414, −1, 1 and 1.414 times 2 mJy beam^{-1}. The central velocity of each channel is labeled. For spatial reference a continuum map of the same area, also with an angular resolution of 50 mas, is shown in the top left hand panel. The contour levels on this continuum image are $\sqrt{2}$ times 3 mJy bm^{-1}.

4.546 GHz at 50 mas angular resolution is $\alpha^{1.3}_{4.5}$ =0.11, using $S_\nu \propto \nu^{-\alpha}$. This value is flat compared to that reported by Akujor et al. between 15 and 22 GHz ($\alpha^{15}_{22} = -1.05$). The steeply inverted spectral index of $\alpha \approx -1$ can be inferred to extend down to 5 GHz when Akujor et al's high frequency observations are compared with their 5 GHz observations and new MERLIN 4.5 GHz observations. The apparent flattening of the spectrum between 1.3 and 4.5 GHz compared to higher frequencies, which is inferred from these observations, is probably due to contributions to the derived 1.3 GHz flux density of this component by more diffuse non-nuclear radio emission from the inner jet. These contributions will become more significant in lower frequency observations since radio jets typically have a spectrum which steepens as the synchrotron emitting particles in the jets age. In fact, if the true radio spectral index of the core component is assumed to be −1 then from the 5 GHz flux densities observed this would imply an expected compact core flux density at 1.3 GHz of ∼7 mJy. In our highest resolution (30 mas) images presented here the fitted core flux density is 13.5 mJy, which implies either a break in the spectrum of the radio core at theses frequencies or, more likely, that even with the 25 pc linear resolution of these observations, that approximately half of the recorded core flux density arises from contributions from unresolved jet components. Multi-frequency, VLBA continuum observations of the core of 3C 293 have been proposed to isolate the core component from extended jet emission in the central tens of parsec.

It is also probable that the 1.3 GHz flux density contribution of the core component is further reduced by free-free absorption resulting from intervening ionised gas expected to surround the AGN upon scales of $<$ 1 pc. In fact free-free absorption is observed in radio spectra of the cores of many active galaxies, for example in many Seyfert nuclei (*e.g.* Gallimore et al. 1999; Pedlar et al. 1998) and in similarly gas-rich radio galaxies (*e.g.* 3C 305; Jackson et al. 2003) at frequencies $\lesssim$1.4 GHz. This implies that in these 1.3 GHz observations the majority of the measured core flux density is contributed by the jet emission rather than the true core.

4.2 Inner jet structure and relative geometry of the radio jet

The jet structure on sub-arcsecond angular resolution scales has been discussed in detail by several authors (*e.g.* Bridle et al. 1981; Akujor et al. 1996; Beswick et al. 2002). However the observations of the inner kiloparsec region of the jet presented here provides the highest angular resolution image of the inner jet region at any frequency. The spectral indices of the brightest jet components between 1.3 and 4.5 GHz are listed in Tab. 2. With the exception of the core (discussed above), these do not have inverted spectra and fall within the range of 0.5→1. There are no significant spectral index gradients detected along the path of the jet, however the western jet components tend to have somewhat steeper spectral indices. At ∼GHz frequencies the radio spectrum of a jet is affected by free-free absorption due to intervening ionised material along the line of sight to the observer and by spectral ageing of electrons along the jet. Thus the slight steepening of the spectral index against the western side of

Table 3. Summary of HI absorption line properties. All velocities are quoted in the optical heliocentric convention and have been obtained from Gaussian fits to the spectral lines. Column densities have been calculated using $1.823\times10^{20}\,\frac{T_{spin}}{100\,K}\int\tau\,dV$. In the following table and discussion throughout this paper we assume a spin temperature of 100 K. Limits upon the detected HI opacity detected in the 30 mas data-set with a detection threshold of 3σ on the spectra averaged over an area of a few beams.

Component	R.A. (J2000) $13^{h}52^{m}$	Dec. (J2000) $31^{\circ}\,26'$	Velocity (V_c) km s^{-1}	FWHM (δV) km s^{-1}	τ (peak)	N_H $\times10^{20}$ atoms cm^{-2}
1	17.ˢ921	46.″35	-	-	<0.07	-
2(E1)	17.913	46.48	13497	52	0.132	6.9
3	17.905	46.44	13496	28	0.205	8.5
4	17.900	46.38	13485	33	0.124	5.2
5(E2)	17.895	46.34	13482	49	0.227	11.4
6(E3)	17.873	46.36	-	-	<0.06	-
7(Core)	17.800	46.48	13478	108	0.185	22.4
8(W1)	17.791	46.56	13365, 13458	90, 71	0.116	19.1
9	17.785	46.60	13338, 13454	134, 135	0.120	19.6
10	17.781	46.60	13356	61	0.105	10.0
11(W2)	17.773	46.59	13383, 13496	169, 85	0.096	16.2
12	17.767	46.56	13313, 13441	54, 28	0.091	11.7
13	17.763	46.53	13310, 13441	54, 28	0.139	29.0

the jet can be interpreted as an increase in free-free absorbing material in front of this half of the source compared to the eastern side, superimposed upon any spectral ageing effects. This interpretation is likely to be a consequence of generally higher gas columns against the western side of the source. This is consitent with the western jet receding as proposed by Beswick et al. and Akujor et al. and supported by the detection of one-sided optical jet emission in K-band *NICMOS* images (Leahy et al. 1999) which is coincident with the radio emission from components E1, E2 and E3.

Assuming that the sub-kpc scale jets are intrinsically symmetric and are moving with relativistic velocities, the size of the counter-jet emission (western side) is expected to appear smaller than that of the jet emission. From the jet counter-jet arm ratio (see *e.g.* Giovannini et al. 1998; Taylor and Vermeulen 1997) estimated from the image in Fig. 3 (lower panel), we derive $\beta\cos\theta\sim0.55$ where β is v/c, v is the jet bulk velocity, and θ is the jet orientation with respect to the line of sight.

The large gap between the core and E3 could be due to non-continuous activity of the central AGN (but no gap is visible on the western side) or more likely to a Doppler de-boosting effect. If the jet velocity is $\sim$0.995c as found in other low and high power radio galaxies (see *e.g.* Giovannini et al. 2001), the observed arm ratio implies $\theta\sim55^{\circ}$ and the Doppler factor is =0.2. With this low value, the observed jet brightness is too faint to be visible. In this scenario the extended emission (E1, E2, E3, W1, and W2) is not the image of the fast jet itself but low velocity shear layer emission surrounding the fast jet spine. This interpretation is in agreement with the large transversal size of the visible emission and with the brightness symmetry of E and W components. The presence of a velocity structure in an intermediate jet region (from the pc to the kpc scale) is expected by the model proposed by Laing (1996) and related to the jet interaction with a dense ISM (Giovannini 2003).

Upon larger scales, as shown in Fig. 2, the $\sim$10 kiloparsec scale jet of 3C 293 has a P.A.$\sim45^{\circ}$. The apparently discordant trajectories of the inner and outer jet structures imply a large position angle change of the jet during this radio galaxy's lifetime. This position angle change probably implies that the radio emission from 3C 293 has gone through two more outbursts and that the younger radio emission observed from the inner jet might be a signature of the radio emission from 3C 293 being 'born again' (Akujor et al 1996). In this case the large scale jet emission would the remnant of older outbursts while the bright inner jet emission is the result of an outburst of order 10^{5} years old. The trigger for this latter outburst, possibly 3C 293's interaction with its nearby companion, may also have affected the alignment of the radio emission from this latter outburst.

5 PROPERTIES OF THE NEUTRAL HYDROGEN ABSORPTION

As has previously been noted by Beswick et al. (2002), the distribution of HI absorption against the central jet within 3C 293 can be broadly split into two differing gas components on the basis of the absorption line widths and spatial distribution. As such, these two components can be treated separately since they trace two different gas distributions and at the resolution of these observations are spatially separated.

5.1 Narrow HI absorbing component: gas in front of the eastern jet

Against the eastern jet the HI absorption lines have a narrow velocity width ($\sim$40 km s^{-1} see Tab. 3) centred at $\sim$13500 km s^{-1} with no broad absorption lines detected against this part of the source. Narrow HI absorption lines are often considered to be indicative of absorption that is the result of ambient gas and hence are often attributed to gas lying at some distance from the centre of the galaxy. In the case of 3C 293 this is the most plausible explanation for the location of the narrow HI absorbing gas seen in front of the eastern jet. In Fig. 7 the areas of highest HI opacity are clearly shown to approximately follow a strip with a P.A. of ∼35°. This distribution is, within astrometric errors, co-spatial with the area of increased HI optical depth observed in lower resolution MERLIN HI absorption observations, associated with the location of foreground dust obscuration observed in *HST* images (see figure 4 & section 4.1 of Beswick et al. 2002).

As can be seen from the absorption spectra (Fig. 4) and the channel maps presented in Fig. 6, the velocity structure narrow absorption is only spread over a few channels. However even with the velocity resolution afforded by these observations (∼28.8 km s^{-1} channel^{-1}) it can be seen in Fig. 7 that the narrow absorption traces a small but distinct velocity gradient of ∼50 km s^{-1} arcsec^{-1} in an approximately south-west to north-east direction. This velocity gradient is also evident in the Gaussian fitted central velocities of the spectra (Tab. 3) and in Fig. 6. This observed velocity gradient is only traceable over an area of a few tenths of an arcsecond (limited by the background continuum extent) but is consistent with the shallow HI absorption velocity gradient (∼46 km s^{-1} arcsec^{-1}) observed over several arcseconds at lower resolution by Beswick et al. (2002). Additionally, this shallow HI structure is consistent with the velocity gradients in ionised gas (∼44 km s^{-1} arcsec^{-1} along a PA∼60→65°) found using long-slit optical observations of [OII] and [OIII] emission lines by van Breugel et al. (1984). Van Breugel et al's observations of the optical ionised gas traced this ∼44 km s^{-1} arcsec^{-1} velocity gradient across the optical extent of 3C 293 out to radii of ∼10″, well beyond the inner radio jets mapped in this experiment.

The co-spatial nature of the narrow HI absorbing material against the eastern jet with a foreground dust lane, along with its consistent velocity structure compared to the optical emission line gas, implies that all three of these components within the ISM of 3C 293 are associated and probably undergoing the same rotation. Considering that the velocity gradients observed in both the narrow HI absorbing and the optical emission line components are consistent and the physical extent over which the optical velocity gradient is observed (out to a radius ∼10″∼8 kpc), it is reasonable to conclude that both of these components, along with the dust lanes, follow the galaxy's rotation. Consequently it can be concluded that the dust, ionised gas and narrow HI absorption are situated on the nearside of the galaxy at a radius of ∼8 kpc and hence are not directly involved in the fuelling of the central activity.

5.2 Broad HI absorbing component: gas in front of the core and western jet

Against the western portion of the VLBI scale jet structure, relatively broad and complex HI absorption is traced (Figs. 5 & 8). As we have discussed in section 4.2 the western jet is more deeply embedded within the host galaxy than the eastern components and is viewed through higher HI gas column densities than the eastern jet.

The velocity structure of the HI absorption against this portion of the source is complex, as seen in the position velocity diagrams (Fig. 8). It should initially be noted that the velocity structure highlighted in this figure only represents a relativity small region of gas in front of the radio continuum structure. However, Fig. 8 does show some structure within the absorbing gas, especially in the lower (80 and 50 mas) angular resolution parts where both the absorbing gas and illuminating continuum are less resolved. These velocity structures become even more apparent in still lower resolution study of this source, such as figure 6 of Beswick et al. (2002). This HI velocity distribution can be interpreted in at least two ways. One interpretation of the data presented is that the velocity structure against the western half of the source is the result of two gas systems centred at ∼13325 and 13500 km s^{-1} respectively. An alternative hypothesis is that the absorption traces a velocity gradient in the gas in front of the AGN and sub-kiloparsec scale jet, along with some gas clouds red or blueshifted away from this velocity gradient.

5.2.1 *The complex, broad absorption as two separate gas components?*

First, let us consider the hypothesis that the observed absorption against the core and western part of the inner radio jet in 3C 293 is composed of two gas systems at different velocities. In this scenario the two gas structures are situated along the line of sight to western half of the source at an undetermined distance from nucleus. This interpretation provides some explanation for the velocity structures observed in Fig. 8 and, to a lesser extent, those observed in figure 6 of Beswick et al. (2002). The velocity structure seen in Fig. 8 and in the Gaussian fits of spectra 8, 9, 10 and 11 in Table. 3 can be satisfactorily fitted by two unassociated absorbing gas structures in the line of sight to the western jet and as such this must be the first explanation considered.

In section 5.1 the narrow absorbing component against the eastern jet was discussed and interpreted to most likely be the result of ambient gas situated toward the nearside of the host galaxy. This component was shown to posses a small velocity gradient of ∼50 km s^{-1} arcsec^{-1}. If it is assumed that this narrow component continues across the entire source, as is reasonable if this gas is associated with gas situated away from the centre of the source, this velocity gradient would imply that a narrow absorption component with a velocity of ∼13430, 13422 and 13410 km s^{-1} at positions core (7), W1(8) and W2(11) respectively should be observed. Although these velocity components are not directly matched by HI absorbing components fitted to the spectra against the western jet (Table 3) small variations in the gradient between the eastern and western halves of the source could be invoked in order to make the velocities consistent. In this scenario the narrow absorption could account for one of the two composite gas structures that are observed against the western jet, with one other velocity component required to replicate the observed structure. This second velocity component can thus be accounted for by either gas localised toward the western jet or, more probably gas situated closer to the western jet and core structure in order that the projected angle of the inner jet (see section 4.2) results in the radio continuum components E1, E2 or E3 lying in front of the gas and thus not illuminating it.

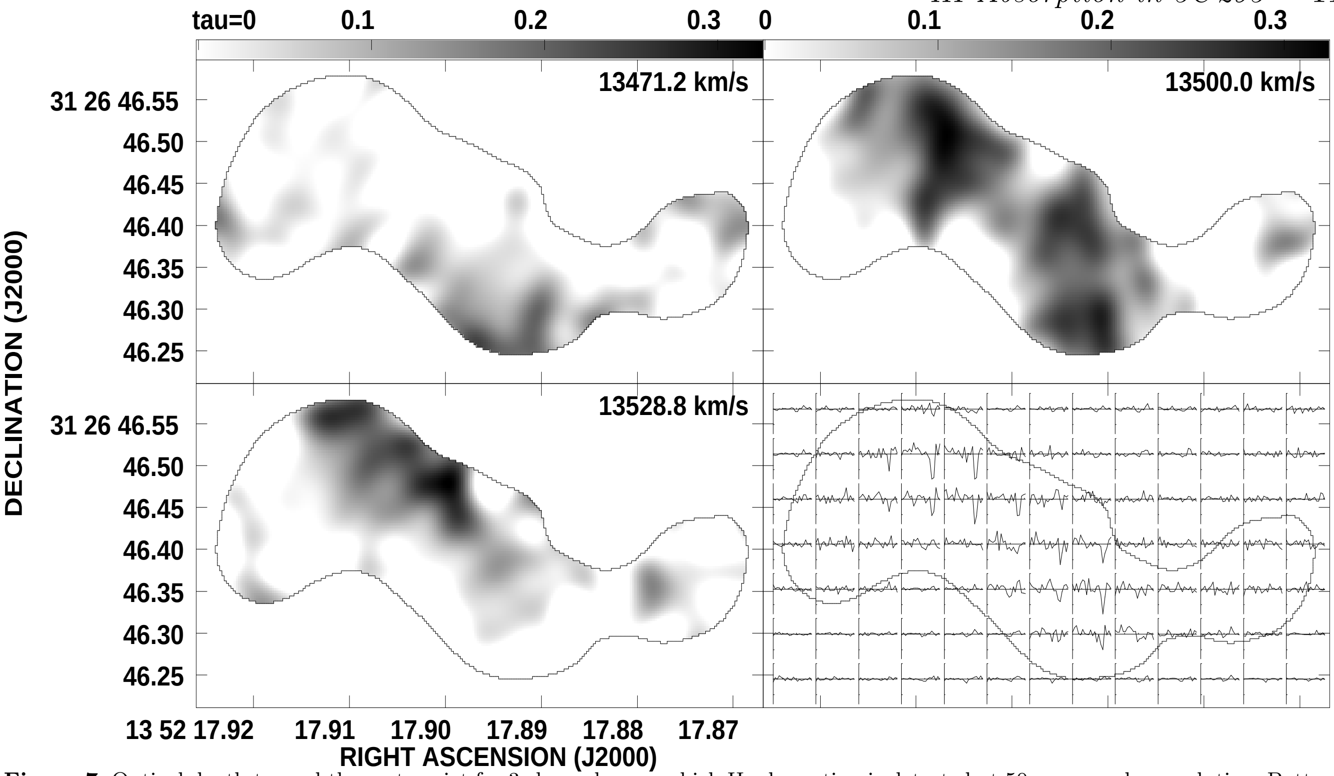

Figure 7. Optical depth toward the eastern jet for 3 channels over which HI absorption is detected at 50 mas angular resolution. Bottom right hand panel shows a grid of HI spectra plotted against position for the same area as the associated channel maps. Each spectrum is plotted as flux density on a scale of -10 to 5 mJy/beam against velocity over the range 13200 to 13600 km s^{-1}. Note that the ridge of higher HI opacity is aligned with a dust lane shown in *HST* observations (see figure 4 of Beswick et al. 2002, dust lane labeled no. 1).

5.2.2 The complex, broad absorption as part of a rotating gas system?

The broad and complex absorption against the western jet can also be interpreted as tracing gas in rotation about the nucleus of the galaxy.

At resolutions of $\sim$1 arcsec, Haschick & Baan (1985) only marginally resolved the radio continuum in the core region of 3C 293 into a two-component structure. Haschick & Baan identified the first of these components with several high optical depth absorption components ($\tau > 0.04$) which trace a velocity gradient of 83 km s^{-1} arcsec^{-1}. This was interpreted as rotation of gas within a disk or ring. With a factor of $\sim$7 higher resolution, Beswick et al. (2002) also traced and began to resolve a still steeper gradient of 179 km s^{-1} arcsec^{-1} centred on the AGN. These conclusions are also supported by OVRO CO observations of a rotating asymetric ring of molecular gas surrounding the nuclear region (Evans et al. 1999). These lower resolution observations imply the existance of some form of rotating gas toward the centre of 3C 293.

If the results presented in this paper are also considered to trace gas rotating about the core as observed at lower resolution by Haschick & Baan (1985), Evans et al. (1999) and Beswick et al. (2002), a similar, although a still steeper, velocity gradient might be expected to be observed. In this scenario the HI absorption against the western jet and core should partially trace any gas rotating about the galaxy centre. If this is the case the best fit for these observations is a gradient of $\sim$410 km s^{-1} arcsec^{-1} centred upon the core and observed against a small area of the radio jet (see Fig. 8).

Assuming that this steep velocity gradient is real, is it the inner part of the same rotating gas structure observed by both Haschick & Baan's and Beswick et al. in HI and Evans et al. in CO? Considering the angular resolution of both Haschick & Baan's and Beswick et al's previous experiments it is probable that, if they were observing the same rotating ring of neutral gas, the angular resolution of their experiments will have smeared the rotational velocities observed. This effect will have resulted in them only observing a lower limit in true velocity gradient. If the gradient observed here is real these even higher angular resolution HI absorption observations trace a steeper velocity gradient, equivalent to 0.34 km s^{-1}pc^{-1}. Unfortunately due to the lack of background radio continuum adjacent to the eastern side of the core this velocity gradient can only be traced over a few hundred parsecs against the core and the western lobe. Assuming the velocity gradient traced in Fig. 8 is just a section of the inner part of an inclined rotating disk of neutral gas and that the disk is centred upon the core component, a dynamical lower limit upon the enclosed mass within a radius of 400 pc of $1.7 \times 10^9 (\sin^{-2} i) \cos^{-1}\theta\, M_\odot$ can be calculated, where i represents the inclination of the assumed disk and θ is the angle between the major axis of the ring/disk and the axis over which the position-velocity diagram has been average (east-west). This value compares well with that derived over a larger radius by Beswick et al. (2002).

The presence of a ring of neutral gas inferred from HI absorption observations has been reported in several previous cases in both radio galaxies (*e.g.* NGC 4261, van Langevelde et al. 2000 and 1946+708, Peck, Taylor & Conway 1999) and Seyfert galaxies (Gallimore et al. 1999) ranging in size from a few tens of parsecs to a 100 or more

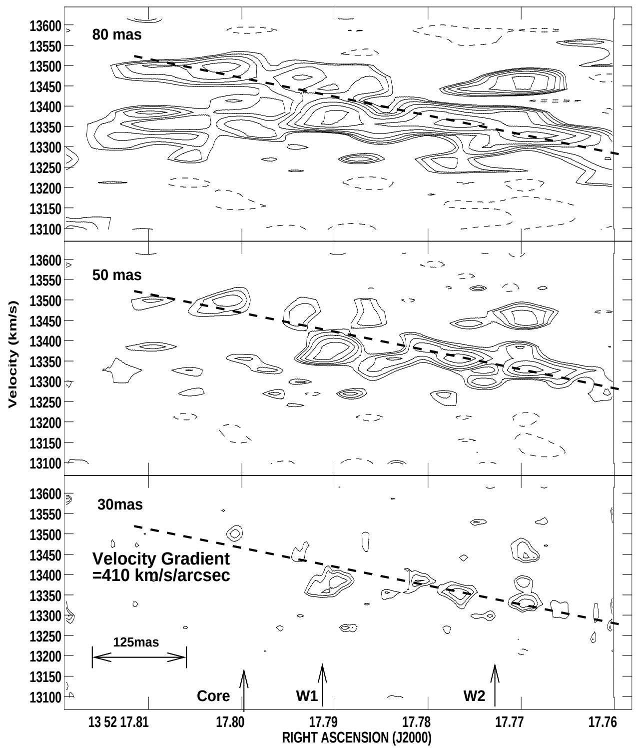

Figure 8. Multi-resolution position-velocity plots of HI absorption against the western jet component at the centre of 3C 293. Contour levels for all three plots are −16, −11.31, −8, −5.657, −4, −2.828, −2, −1.414, −1 & 1 times 0.4 mJy beam^{-1}. In each of these diagrams the absorption signal has been averaged over the declination range of the continuum source. The spatial angular resolution of the spectral line cubes that each of these position velocity plots have been extracted from is labelled in the top left hand corner of each plot. The dashed line shown on all three plots represents a velocity gradient of 410 km s^{-1} arcsec^{-1}. The spatial position of radio continuum components labelled in Fig. 3 are also shown by arrows positioned along the bottom plot.

parsecs. Although the circumnuclear ring of HI inferred in 3C 293 is considerably larger in extent than many other such examples, it has been traced over a very wide range of scales from few tens of parsecs out to greater than half a kiloparsec thus overlapping with the disk scales previously observed in similar sources. This circumnuclear ring or disk of neutral gas appears to be situated within the radius of an asymmetric molecular gas ring detected in CO emission and absorption (Evans et al. 1999). Evans et al. determined the radius of the molecular disk to be ∼2.8 kpc and containing $\sim 10^{11}(\sin^{-2}i)\,\mathrm{M}_{\odot}$ of material within this radius with ∼10% of this mass made up of molecular gas. In these senses the neutral and molecular gas structures appear to mimic an ‘onion-skin’ model in which a region of ionised gas surrounds the AGN, and in turn is encompassed by a ring of neutral gas beyond which lies the molecular gas. This model has been successfully used to explain the gas structure of nuclear regions of Seyfert galaxies (*e.g.* Mundell et al. 2003) albeit in lower power AGN and on much smaller scales.

5.3 Relationship of nuclear absorpion with gas inflows and outflows: interaction of the eastern jet with the ISM

In the last few years one of the most interesting observational HI absorption results to emerge has been the detection of incredibly broad, low optical depth, blue-wings in the absorption spectra of some active galaxies (*e.g.* Oosterloo et al. 2000; Morganti et al. 2003). In particular, Morganti et al, using the WSRT observed a ∼1000 km s^{-1} blue-shifted wing to the already broad HI absorption detected against the central ten kiloparsecs of 3C 293. This broad HI absorption with typical opacities of ∼0.15% interpreted to be the result of outflows of gas from the central region, which are probably driven by interactions between the radio plasma and the ISM. Without the angular resolution to determine which part of the complex radio jet structure (see Fig. 3) illuminates and/or interacts with this ISM component, Morganti et al. inferred from the location of the broad optical emission lines (coincident with the eastern jet components in Fig. 3) that it is probable that broad HI also originates from in the vicinity of E1, E2 and E3 components. As has already been discussed, we surmise that this portion of the radio jet is approaching, and it is also the location of a reported optical jet feature (Leahy et al. 1999). The trajectory of this portion of the jet, along with its location buried deep within a dust lane in the central few kiloparsecs of the host galaxy do support their hypothesis. Additionally as we describe in section 4.1.2 the radio jet emission observed is consistent not with a fast jet but with emission from a low velocity shear layer surrounding the faster jet spine. This may provide an environment in which a jet-ISM interaction can occur and accelerate material to the high velocities seen by Morganti et al. whilst also allowing regions to cool and recombine to become neutral while moving at high velocities. This part of the inner jet in 3C 293 has previously been suggested as the site for probably jet-ISM interactions and the entrainment of gas by van Breugel et al. (1984). Unfortunately neither the observations presented here or those presented in Beswick et al. (2002) have the sensitivity or sufficient bandwidth to confirm the broad HI absorption detected with WSRT and hence cannot be used to categorically pinpoint the spatial location of this blue-shifted gas. However it is clear that this broad absorption component is probably not related to the relatively narrow and deep nuclear absorption detected in this and by previous HI observations of this source (*e.g.* Haschick & Baan 1985; Beswick et al. 2002).

6 CONCLUSIONS

We have used observations made using the VLA including Pie Town, MERLIN and global VLBI to study the 1.3 GHz radio continuum structure of the central kiloparsec of the peculiar radio galaxy 3C 293 and to investigate the kinematics and the distribution of HI via absorption against this radio continuum.

We confirm the component identified originally by Akujor et al. (1996) as the most probable site of the central engine and place limits upon its size of $\lesssim$17 pc. Using both MERLIN 4.5 GHz data (Akujor et al. 1996) and new high resolution 1.3 GHz observations presented here we determine a radio spectral index of $\alpha_{4.5}^{1.3}$ =0.11 for the core component. We discuss in detail the differences in the value of this spectral index compared to that derived for the same component at higher radio frequencies ($\alpha_{22}^{15} \approx -1$; Akujor et al. 1996). It is concluded the flat spectral index derived in this study may be affected by a significant amount of unresolved radio emission from the jet close to the AGN and that this has been incorporated in our 1.3 GHz flux density measurement of the component resulting in the observed flat spectrum. In addition to the core we have mapped the radio continuum emission of the jet in 3C 293 across a variety of angular scales. From this multi-scale approach it is apparent that the trajectory of the radio jet emission in 3C 293 has changed significantly over the source's lifetime. In this region, observational data suggest the presence of an intrinsically symmetric jet with a highly relativistic spine, surrounded by a low velocity shear layer because of the jet interaction with the dense ISM. The jet orientation with respect to the line of sight is ∼50° with the eastern jet approaching us.

Extensive HI absorption has been detected against both the eastern and western jet components within the central kiloparsec of 3C 293, consistent with lower angular resolution studies by Haschick & Baan (1985) and Beswick et al. (2002). As was previously known, the structure of the HI absorption against the eastern jet components primarily consists of strong and narrow features with a small velocity gradient whereas the absorption against the western and core components are much broader.

The narrow HI absorption detected against the eastern radio jet traces a small velocity gradient of ∼ 50 km s^{-1} arcsec^{-1}, consistent with the velocity gradient observed in ionised gas by van Breugel et al. (1984). Additionally we have re-confirmed (following Beswick et al. 2002) that this narrow HI absorption is co-spatial with the location of dust lanes observed by the *HST*. From the association of these three components we conclude that they are all most likely situated ∼8 kpc from the central part of the galaxy and are all probably undergoing galactic rotation.

Against the western radio jet and core complex HI absorption is also detected. This absorption is discussed in terms of either tracing two gas structures at undetermined distances along the line of sight to the jet or a steep velocity gradient which may be interpreted as neutral gas in rotation about the core. If this is interpreted as rotation by a gas disk, it would imply an enclosed mass of at least 1.7×10^9 solar masses within a radius of 400 pc of the core.

ACKNOWLEDGMENTS

RJB acknowledges PPARC support. ABP thanks the staff of Jodrell Bank Observatory for their hospitality, and acknowledges support from MPIfR during this project. We would also like to thank J. P. Leahy for useful discussions about this project and allowing us access to his data prior to publication. We thank A. Pedlar for his numerous contributions to the earlier stages of this project and encouragement throughout. The authors also thank the referee for many useful comments that have helped to improve the content and structure of this publication.

The VLA and VLBA are operated by the National Radio Astronomy Observatory. The National Radio Astronomy Observatory is a facility of the National Science Foundation operated under cooperative agreement by Associated Universities, Inc. MERLIN is a national facility operated by the University of Manchester on behalf of PPARC in the UK. The European VLBI Network is a joint facility of European, Chinese, South African and other radio astronomy institutes funded by their national research councils.

REFERENCES

Akujor C. E., Leahy J. P., Garrington S. T., Sanghera H., Spencer R. E., Schilizzi R. T., 1996, MNRAS, 278, 1
Allen M. G., Sparks W. B., Koekemoer A., Martel A. R., O'Dea C. P., Baum S. A., Chiaberge M., Macchetto F. D., Miley G. K. 2002 ApJS, 139, 411
Baan W. A., Haschick A. D., 1981, ApJ, 243, L143
Beswick R. J., Pedlar, A., Holloway, A. J., 2002, MNRAS, 329, 620
Beswick R. J. 2002, PhD thesis, Univ. Manchester, UK.
Bridle A. H., Fomalont E. B., Cornwell T. J., 1981, AJ, 86, 1294
Cecil G., Bland-Hawthorn J., Veilleux S., Filippenko, A. V., 2001, ApJ, 555, 338
Evans A. S., Sanders D. B., Surace J. A., Mazzarella J. M., 1999, ApJ, 511, 730
Fanaroff B. L., Riley J. M., 1974, MNRAS, 167, 31
Gallimore J. F., Baum S. A., O'Dea C. P., Pedlar A., Brinks E., 1999, ApJ, 524, 684
Giovannini G., Cotton W. D., Feretti L., Lara L., Venturi T., 1998, ApJ, 493, 632
Giovannini G., Cotton W. D., Feretti L., Lara L., Venturi T., 2001, ApJ, 552, 508
Giovannini G., 2003, in *"The Physics of Relativistic Jets in the Chandra and XMM Era",* eds G. Brunetti, D.E. Harris, R.M. Sambruna, G. Setti; New Astronomy Reviews, Vol. 47, p551
Haschick A. D., Baan W. A., 1985, ApJ, 289, 574
Heckman T. M., Illingworth G. D., Miley G. K., van Breugel W. J. M., 1985, ApJ, 299, 41
Jackson N. J., Beswick R. J., Pedlar A., Cole G. H. J., Sparks W. B., Leahy J. P., Axon D. J., Holloway A. J., 2003, MNRAS, 338, 643
Laing R. S., 1996, in *"Energy Transport in Radio Galaxies and Quasars",* eds. Hardee P. E., Bridle A. H., Zensus J. A., Astron. Soc. Pac., Vol. 100, San Francisco, p. 241
Leahy J. P., Sparks W. B., Jackson N. J. F., 1999, AAS, 194, 7304L
Maloney P. R., Hollenbach D. J., Tielens A. G. G. M1996, ApJ, 466, 561
Martel A. R., et al. 1999, ApJS, 122, 81
Morganti R., Oosterloo T. A., Emonts B. H. C., van der Hulst J. M., Tadhunter C. N., 2003, ApJ, 593, L69
Mundell C. G., Wrobel J. M., Pedlar A., Gallimore J. F. 2003, ApJ, 583, 192
Oosterloo T. A., Morganti R., Tzioumis A., Reynolds J., King E., McCulloch P. & Tsvetanov Z. 2000, AJ, 119, 2085
Peck A. B., Taylor G. B., Conway J. E. 1999, ApJ, 521, 103

Pedlar A., Fernandez B., Hamilton N. G., Redman M. P., Dewdney P. E. 1998, MNRAS, 300, 1071
Shostak G. S., van Gorkom J. H. Ekers R. D., Sanders R. H., Goss W. M., Cornwell T. J., 1983, A & A, 119, L3
Taylor G. B., Vermeulen R. C. 1997, ApJ,485, L9
Thomasson P., 1986,QJRAS, 27, 413
van Breugel W., Heckman T., Butcher H., Miley G., 1984, ApJ, 277, 82
van Langevelde H. J., Pihlström Y. M., Conway J. E., Jaffe W., Schilizzi R. T., 2000, A & A 354, L45